2010-05

Multistatic Radar Imaging of Moving Targets

Wang, Ling

Multistatic Radar Imaging of Moving Targets

Ling Wang
College of Information Science and Technology
Nanjing University of Aeronautics and Astronautics
Nanjing 210016, China

Margaret Cheney
Department of Mathematical Sciences
Rensselaer Polytechnic Institute
Troy, NY 12180

Brett Borden
Physics Department
Naval Postgraduate School
Monterey, CA 93943-5001

***Abstract*— We develop a linearized imaging theory that combines the spatial, temporal, and spectral aspects of scattered waves. We consider the case of fixed sensors and a general distribution of objects, each undergoing linear motion; thus the theory deals with imaging distributions in phase space. We derive a model for the data that is appropriate for narrowband waveforms in the case when the targets are moving slowly relative to the speed of light. From this model, we develop a phase-space imaging formula that can be interpreted in terms of filtered backprojection or matched filtering. For this imaging approach, we derive the corresponding phase-space point-spread function. We show plots of the phase-space point-spread function for various geometries, and various combinations of waveforms.**

I. Introduction

The use of radar for detection and imaging of moving targets is a topic of great interest. It is well-known that radar signals have two important attributes, namely the time delay, which provides information on the target range, and the Doppler shift, which can be used to infer target down-range velocity. Classical "radar ambiguity" theory [1]–[3] shows that the transmitted waveform determines the accuracy to which target range and velocity can be obtained from a backscattered radar signal. The classical theory, however, does not address the question of what information can be obtained when transmitters and receivers are positioned at different locations. Such a theory is needed to address questions such as

- In a multistatic system, which transmitters should transmit which waveforms?
- How many transmitters are needed, and where should they be positioned?
- How can data from such a system be used to form an image of unknown moving targets?
- What is the resolution (in position and in velocity) of such a system?

Some work has been done to develop such a theory:

- Ambiguity theory for bistatic systems has been developed in [4]–[7]; such systems allow for estimation of only one component of the velocity vector.
- For multistatic systems, the work [8]–[14] developed methods for moving-target *detection*.
- Theory for use of a multistatic system for imaging of a *stationary* scene is well-known; see *e.g.* [15]–[18].
- Multistatic *imaging* of *moving* targets (phase-space imaging) was developed in [19] for the case of fixed transmitters and receivers. This theory combines spatial, temporal, and spectral attributes of radar data; in particular the theory exploits the actual Doppler shift from moving targets.

The work [19] is extended in the present paper, which sets forth the basic ideas in the special cases that are of interest to radar-based imaging, and undertakes numerical exploration of the properties of the imaging system. In this paper we investigate the case when different waveforms are transmitted from different locations. We show that under some circumstances, both the spatial position and (vector) velocities of multiple targets can be found.

This work does *not* address the following issues:

- Distinguishing the part of the received signal that is due to a particular transmitter. This might be accomplished by using quasi-orthogonal codes or using different frequency bands for the different transmitters.
- Accounting for the change in reflectivity of a target when it is viewed at different frequencies or different aspect angles. Here we assume that the target scatters isotropically and that the scattering is frequency-independent.

II. Model for Data

We model wave propagation and scattering by the scalar wave equation for the wavefield $\psi(t,\boldsymbol{x})$ due to a source waveform $s(t,\boldsymbol{x})$ transmitted at time $-T_{\boldsymbol{y}}$ from location $\boldsymbol{y}$:

$$[\nabla^2 - c^{-2}(t,\boldsymbol{x})\partial_t^2]\psi(t,\boldsymbol{x},\boldsymbol{y}) = \delta(\boldsymbol{x}-\boldsymbol{y})s_{\boldsymbol{y}}(t+T_{\boldsymbol{y}})\,. \quad (1)$$

For simplicity, we consider only localized isotropic sources; the work can easily be extended to more realistic antenna models [20].

A single scatterer moving at velocity $\boldsymbol{v}$ corresponds to an index-of-refraction distribution $n^2(\boldsymbol{x}-\boldsymbol{v}t)$:

$$c^{-2}(t,\boldsymbol{x}) = c_0^{-2}[1+n^2(\boldsymbol{x}-\boldsymbol{v}t)]\,, \quad (2)$$

where c_0 denotes the speed in the stationary background medium (here assumed constant). For radar, c_0 is the speed of light in vacuum. We write $q_{\boldsymbol{v}}(\boldsymbol{x}-\boldsymbol{v}t) = c_0^{-2}n^2(\boldsymbol{x}-\boldsymbol{v}t)$. To model multiple moving scatterers, we let $q_{\boldsymbol{v}}(\boldsymbol{x}-\boldsymbol{v}t)\,\mathrm{d}^3x\,\mathrm{d}^3v$ be the corresponding quantity for the scatterers in the volume $\mathrm{d}^3x\,\mathrm{d}^3v$ centered at $(\boldsymbol{x},\boldsymbol{v})$. In other words, q is a distribution in *phase space*, and $q_{\boldsymbol{v}}$ is the spatial distribution, at time $t=0$, of scatterers moving with velocity $\boldsymbol{v}$. Consequently, the scatterers in the spatial volume d^3x (at $\boldsymbol{x}$) give rise to

$$c^{-2}(t,\boldsymbol{x}) = c_0^{-2} + \int q_{\boldsymbol{v}}(\boldsymbol{x}-\boldsymbol{v}t)\,\mathrm{d}^3v\,. \quad (3)$$

978-1-4244-5813-4/10/$26.00 ©2010 IEEE

Report Documentation Page

Form Approved
OMB No. 0704-0188

1. REPORT DATE	2. REPORT TYPE	3. DATES COVERED
MAY 2010		**00-00-2010 to 00-00-2010**

4. TITLE AND SUBTITLE	5a. CONTRACT NUMBER
Multistatic Radar Imaging of Moving Targets	5b. GRANT NUMBER
	5c. PROGRAM ELEMENT NUMBER
6. AUTHOR(S)	5d. PROJECT NUMBER
	5e. TASK NUMBER
	5f. WORK UNIT NUMBER
7. PERFORMING ORGANIZATION NAME(S) AND ADDRESS(ES) **Naval Postgraduate School,Physics Department,Monterey,CA,93943**	8. PERFORMING ORGANIZATION REPORT NUMBER
9. SPONSORING/MONITORING AGENCY NAME(S) AND ADDRESS(ES)	10. SPONSOR/MONITOR'S ACRONYM(S)
	11. SPONSOR/MONITOR'S REPORT NUMBER(S)

12. DISTRIBUTION/AVAILABILITY STATEMENT
Approved for public release; distribution unlimited

13. SUPPLEMENTARY NOTES
See also ADM002322. Presented at the 2010 IEEE International Radar Conference (9th) Held in Arlington, Virginia on 10-14 May 2010. Sponsored in part by the Navy.

14. ABSTRACT
We develop a linearized imaging theory that combines the spatial, temporal, and spectral aspects of scattered waves. We consider the case of fixed sensors and a general distribution of objects, each undergoing linear motion; thus the theory deals with imaging distributions in phase space. We derive a model for the data that is appropriate for narrowband waveforms in the case when the targets are moving slowly relative to the speed of light. From this model, we develop a phase-space imaging formula that can be interpreted in terms of filtered backprojection or matched filtering. For this imaging approach we derive the corresponding phase-space point-spread function. We show plots of the phase-space point-spread function for various geometries, and various combinations of waveforms.

15. SUBJECT TERMS

16. SECURITY CLASSIFICATION OF:			17. LIMITATION OF ABSTRACT	18. NUMBER OF PAGES	19a. NAME OF RESPONSIBLE PERSON
a. REPORT **unclassified**	b. ABSTRACT **unclassified**	c. THIS PAGE **unclassified**	**Same as Report (SAR)**	**6**	

We note that the physical interpretation of $q_{\boldsymbol{v}}$ involves a choice of a time origin. A choice that is particularly appropriate, in view of our assumption about linear target velocities, is a time during which the wave is interacting with targets of interest. This implies that the activation of the antenna at $\boldsymbol{y}$ takes place at a negative time which we denote by $-T_{\boldsymbol{y}}$. The wave equation corresponding to (3) is then

$$\left[\nabla^2 - c_0^{-2}\partial_t^2 - \int q_{\boldsymbol{v}}(\boldsymbol{x}-\boldsymbol{v}t)\,\mathrm{d}^3v\,\partial_t^2\right]\psi(t,\boldsymbol{x}) = s_{\boldsymbol{y}}(t+T_{\boldsymbol{y}})\delta(\boldsymbol{x}-\boldsymbol{y})\,. \quad (4)$$

With the Born (single-scattering) approximation and far-field approximation, the he scattered field can be written [19]

$$\psi_{\mathrm{f}}^{\mathrm{sc}}(t,\boldsymbol{z},\boldsymbol{y}) = \int \frac{\ddot{s}_{\boldsymbol{y}}\left[\phi(\boldsymbol{x},\boldsymbol{v})\right]}{(4\pi)^2|\boldsymbol{z}||\boldsymbol{y}|} q_{\boldsymbol{v}}(\boldsymbol{x})\,\mathrm{d}^3x\,\mathrm{d}^3v \quad (5)$$

where

$$\phi(\boldsymbol{x},\boldsymbol{v}) = \alpha_{\boldsymbol{v}}\left(t - |\boldsymbol{z}|/c + \hat{\boldsymbol{z}}\cdot\boldsymbol{x}/c\right) - |\boldsymbol{y}|/c + \hat{\boldsymbol{y}}\cdot\boldsymbol{x}/c + T_{\boldsymbol{y}} \quad (6)$$

and where α denotes the Doppler scale factor

$$\alpha_{\boldsymbol{v}} = \frac{1+\widehat{\boldsymbol{y}}\cdot\boldsymbol{v}/c}{1-\widehat{\boldsymbol{z}}\cdot\boldsymbol{v}/c} \quad (7)$$

In the case when $|\boldsymbol{v}|/c \ll 1$, we have $\alpha_{\boldsymbol{v}} \approx 1 + (\hat{\boldsymbol{y}}+\hat{\boldsymbol{z}})\cdot\boldsymbol{v}/c$.

To write (5) as a Fourier Integral Operator, we write $s_{\boldsymbol{y}}(t)$ in terms of its inverse Fourier transform:

$$s_{\boldsymbol{y}}(t) = \frac{1}{2\pi}\int \mathrm{e}^{-\mathrm{i}\omega' t} S_{\boldsymbol{y}}(\omega)\,\mathrm{d}\omega'\,. \quad (8)$$

We note that by the Paley-Weiner theorem, S is analytic since it is the inverse Fourier transform of the finite-duration waveform s. With (8), we convert (5) into

$$\psi_{\mathrm{f}}^{\mathrm{sc}}(t,\boldsymbol{z},\boldsymbol{y}) = \int \frac{(-\mathrm{i}\omega)^2}{(4\pi)^2|\boldsymbol{z}||\boldsymbol{y}|}\exp\Big(-\mathrm{i}\omega\left[\phi(\boldsymbol{x},\boldsymbol{v})\right]\Big) S_{\boldsymbol{y}}(\omega)\,\mathrm{d}\omega q_{\boldsymbol{v}}(\boldsymbol{x})\,\mathrm{d}^3x\,\mathrm{d}^3v. \quad (9)$$

III. Image Formation

The corresponding imaging operation is a filtered version of the formal adjoint of the "forward" operator $\mathcal{F}$. Thus we form the phase-space image $I(\boldsymbol{p},\boldsymbol{u})$ as

$$I_\infty(\boldsymbol{p},\boldsymbol{u}) = \int \mathrm{e}^{\mathrm{i}\omega[\phi(\boldsymbol{p},\boldsymbol{u})]} Q_\infty(\omega,\boldsymbol{p},\boldsymbol{u},\boldsymbol{z},\boldsymbol{y})\,\mathrm{d}\omega\, \psi^{\mathrm{sc}}(t,\boldsymbol{z},\boldsymbol{y})\,\mathrm{d}t\,\mathrm{d}^n z\,\mathrm{d}^m y. \quad (10)$$

The specific choice of filter is dictated by various considerations [21], [22]; here we make choices that connect the resulting formulas with familiar theories. We take the filter to be

$$Q_\infty(\omega,\boldsymbol{p},\boldsymbol{u},\boldsymbol{z},\boldsymbol{y}) = -\frac{(4\pi)^2}{\omega^2}|\boldsymbol{z}||\boldsymbol{y}|S_{\boldsymbol{y}}^*(\omega)J(\omega,\boldsymbol{p},\boldsymbol{u},\boldsymbol{z},\boldsymbol{y})\alpha_{\boldsymbol{u}}\,, \quad (11)$$

which leads (below) to the matched filter. Here the star denotes complex conjugation, and J is a geometrical factor [19] that depends on the configuration of transmitters and receivers.

IV. Analysis of the Point-Spread Function

We obtain the point-spread function of the imaging system by substituting (9) into (10). We thus obtain an image

$$I_\infty(\boldsymbol{p},\boldsymbol{u}) = \int K_\infty(\boldsymbol{p},\boldsymbol{u};\boldsymbol{x},\boldsymbol{v}) q_{\boldsymbol{v}}(\boldsymbol{x}) d^3x d^3v \quad (12)$$

Many radar systems use a narrowband waveform, which is of the form

$$s_{\boldsymbol{y}}(t) = \tilde{s}_{\boldsymbol{y}}(t)\,\mathrm{e}^{-\mathrm{i}\omega_{\boldsymbol{y}}t} \quad (13)$$

where $\tilde{s}(t,\boldsymbol{y})$ is slowly varying, as a function of t, in comparison with $\exp(-\mathrm{i}\omega_{\boldsymbol{y}}t)$, where $\omega_{\boldsymbol{y}}$ is the carrier frequency for the transmitter at position $\boldsymbol{y}$. For the narrowband case, we write $K_\infty^{(\mathrm{NB})}$ instead of K_∞.

In the narrowband case, the point-spread function reduces to [19]

$$K_\infty^{(\mathrm{NB})}(\boldsymbol{p},\boldsymbol{u};\boldsymbol{x},\boldsymbol{v}) = -\int \omega_{\boldsymbol{y}}^2 e^{\mathrm{i}\Phi_{\boldsymbol{y},\boldsymbol{z}}}\tilde{J}(\boldsymbol{p},\boldsymbol{u},\boldsymbol{z},\boldsymbol{y}) A_{\boldsymbol{y}}\Big(k_{\boldsymbol{y}}(\hat{\boldsymbol{y}}+\hat{\boldsymbol{z}})\cdot(\boldsymbol{u}-\boldsymbol{v}),\ (\hat{\boldsymbol{z}}+\hat{\boldsymbol{y}})\cdot(\boldsymbol{x}-\boldsymbol{p})/c\Big)\,\mathrm{d}^n z\,\mathrm{d}^m y\,, \quad (14)$$

where $\tilde{J}$ is a geometrical factor closely related to J above, where

$$A_{\boldsymbol{y}}(\tilde{\omega},\tau) = \mathrm{e}^{-\mathrm{i}\omega_{\boldsymbol{y}}\tau}\int \tilde{s}_{\boldsymbol{y}}^*(t-\tau)\,\tilde{s}_{\boldsymbol{y}}(t)\,\mathrm{e}^{\mathrm{i}\tilde{\omega}t}\,\mathrm{d}t\,. \quad (15)$$

is the narrowband ambiguity function (which is defined here to include a phase) and where

$$e^{\mathrm{i}\Phi_{\boldsymbol{y},\boldsymbol{z}}(\boldsymbol{x},\boldsymbol{v},\boldsymbol{p},\boldsymbol{u})} = \exp\left[\mathrm{i}(\tilde{\varphi}_{\boldsymbol{x},\boldsymbol{v}} - \tilde{\varphi}_{\boldsymbol{p},\boldsymbol{u}})\right] \exp\left(-\mathrm{i}k_{\boldsymbol{y}}(\beta_{\boldsymbol{u}} - \beta_{\boldsymbol{v}})(\hat{\boldsymbol{z}}+\hat{\boldsymbol{y}})\cdot\boldsymbol{x}\right) \quad (16)$$

with $k_{\boldsymbol{y}} = \omega_{\boldsymbol{y}}/c$, $\beta_{\boldsymbol{v}} = (\hat{\boldsymbol{y}}+\hat{\boldsymbol{z}})\cdot\boldsymbol{v}/c$, and

$$\begin{aligned}\tilde{\varphi}_{\boldsymbol{x},\boldsymbol{v}} - \tilde{\varphi}_{\boldsymbol{p},\boldsymbol{u}} &= \frac{\omega_{\boldsymbol{y}}}{c}\left[[(1+\beta_{\boldsymbol{u}})\hat{\boldsymbol{z}}+\hat{\boldsymbol{y}}]\cdot\boldsymbol{p} - [(1+\beta_{\boldsymbol{v}})\hat{\boldsymbol{z}}+\hat{\boldsymbol{y}}]\cdot\boldsymbol{x}\right] \\ &= k_{\boldsymbol{y}}\left[(\hat{\boldsymbol{z}}+\hat{\boldsymbol{y}})\cdot(\boldsymbol{p}-\boldsymbol{x}) + \hat{\boldsymbol{z}}\cdot(\beta_{\boldsymbol{u}}\boldsymbol{p} - \beta_{\boldsymbol{v}}\boldsymbol{x})\right]\end{aligned} \quad (17)$$

The narrowband result (14) clearly exhibits the importance of the bistatic bisector vector $\hat{\boldsymbol{y}}+\hat{\boldsymbol{z}}$.

V. Numerical Siimulations of the Point-Spread Function

The point-spread function contains all the information about the performance of the imaging system. Unfortunately it is difficult to visualize this PSF because it depends on so many variables. In the case when the positions and velocities are restricted to a known plane, the PSF is a function of four variables.

We would like to know whether we can find both the position and velocity of moving targets. Ideally, the point-spread function is delta-like, and so we can obtain both position and velocity. If, however, the PSF is ridge-like, then there will be uncertainty in some directions or in some combination of positions and velocities.

In order to look for possible ridge-like behavior, we write the PSF as

$$K_{\infty}^{(\mathrm{NB})}(\boldsymbol{p},\boldsymbol{u};\boldsymbol{x},\boldsymbol{v}) = K(|\boldsymbol{p}|(\cos\theta,\sin\theta),|\boldsymbol{u}|(\cos\phi,\sin\phi),\boldsymbol{x},\boldsymbol{v}). \tag{18}$$

We plot the PSF for a fixed target position $\boldsymbol{x}$ and target velocity $\boldsymbol{v}$. We then sample θ and ϕ at intervals of $\pi/4$, and for each choice of θ and ϕ, we plot $|\boldsymbol{p}|$ versus $|\boldsymbol{u}|$. This process results in $9 \times 9 = 81$ plots of $|\boldsymbol{p}|$ versus $|\boldsymbol{u}|$. Finally, to show the entire four-dimensional space at a glance, we display all the 81 plots simultaneously on a grid, arranged as shown in Fig. 1.

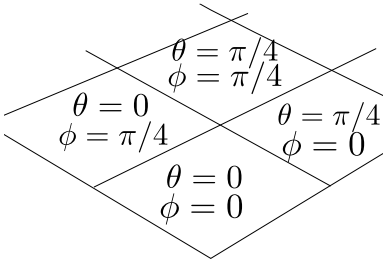

Fig. 1: This shows how our figures display the four-dimensional point-spread function (18).

A. Simulation Parameters

Our strategy in the simulations is to use a delta-like ambiguity function, and investigate the effect of geometry on the overall point-spread function. In all cases, we use a transmit time of $T_{\boldsymbol{y}} = 0$.

- *Waveforms:* Two waveforms of unit amplitude are used. Waveform 1 is a high-range-resolution chirp of duration 9.2×10^{-6} s and bandwidth 200MHz. It is sampled at 250 MHz (2300 sample points).
  Waveform 4 is a single long CW pulse, of duration .05s, sampled at 5 kHz (250 sample points). It has high Doppler resolution.
- *Target Location and Velocity* The target location is (225 m, 45 degrees) and its velocity is (20 m/s, 0 degrees).

B. Examples

a) Two transmitters, one receiver: For the simulation of two transmitters and one receiver, the two transmitters are located at (10000m, 0) and (-10000m, 0), respectively and the receiver is located at (0, 10000m). (See Figure 2.)

The PSFs for a single transmitter and two receivers are shown in Figures 3 through 5. Figure 3 shows the PSF when both transmitters transmit Waveform 1; Figure 4 shows the PSF when both transmitters transmit Waveform 4; and Figure 5 shows the PSF when one transmitter transmits Waveform 1 and the other transmits Waveform 4.

We see that for this geometry, the PSF is ridge-like. Whereas a high-range-resolution waveform provides only range information, it appears that the use of high-Doppler-resolution

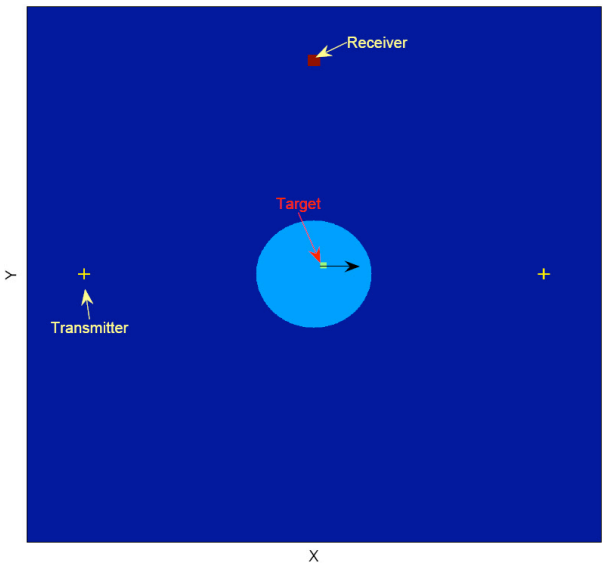

Fig. 2: This shows the geometry for the two-transmitter, single-receiver case, together with the target and region of interest (not to scale).

waveforms may be able to provide not only velocity information but also some range information. The fact that the location ridges (Figs. 3 and 5) are higher than the velocity ridges (Figs. 4 and 5) may be explained by the fact that the total power of (the discretized version of) waveform 1 is greater than that of (the discretized version of) waveform 4. This suggests that balancing the power of the various transmitters may be important.

b) Two Transmitters, Two Receivers: For the two-transmitter, two-receiver case, the two transmitters are located at (10000m, 0) and (0, 10000m) and the two receivers are located at (10000m, 0) and (-10000m, 0), respectively. See figure 6.

Figure 7 shows the combined point-spread function when the transmitter on the x axis transmits waveform 1 and the transmitter on the y axis transmits waveform 4.

Comparing Figures 5 and 7, we see that adding a receiver weakens the ambiguities.

c) Circular geometry: We also considered a circular arrangement of 8 transmitters and 10 receivers. The transmitters are equally spaced around a circle of radius 10000 m; the receivers are equally spaced around a circle of radius 9000 m. (See Figure 8.) The scene of interest has radius 1000 m.

We see from Figure 9 that the velocity information cannot be obtained from the single high-range-resolution waveform.

We note that both the position and the velocity can be resolved well if the same high Doppler-resolution waveform is used for each transmitter.

VI. Conclusions and Future Work

We have developed a linearized imaging theory that combines the spatial, temporal, and spectral aspects of scattered waves.

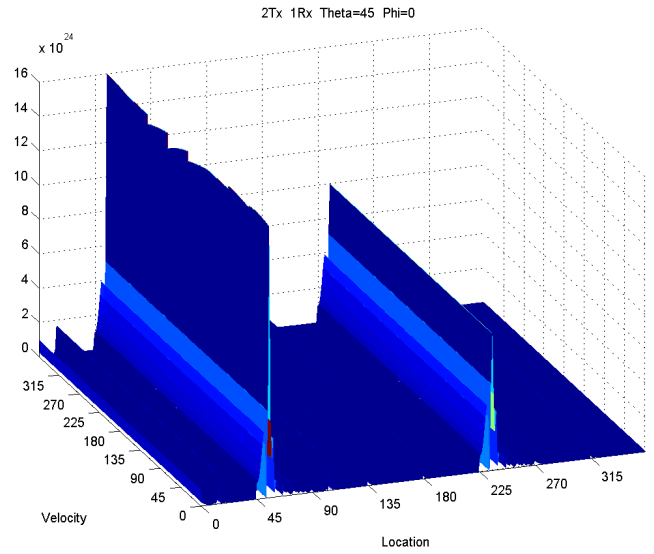

Fig. 3: This shows the combined point-spread function for the two-transmitter, single-receiver case, when both transmitters transmit waveform 1.

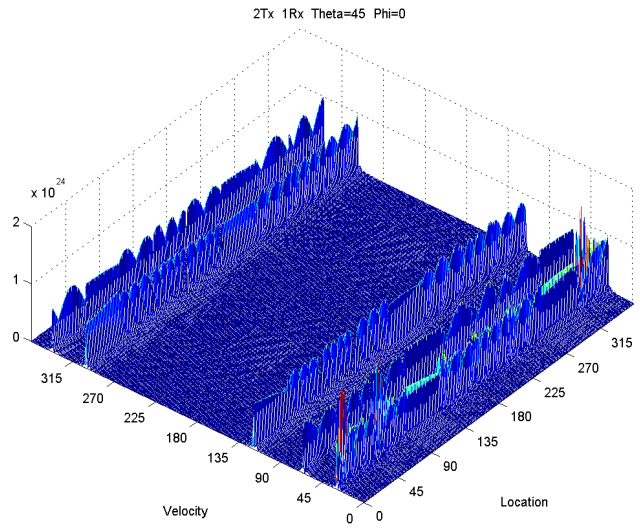

Fig. 4: This shows the combined point-spread function for the two-transmitter, single-receiver case, when both transmitters transmit waveform 4.

This imaging theory is based on the general (linearized) expression we derived for waves scattered from moving objects, which we model in terms of a distribution in phase space. The expression for the scattered waves is of the form of a Fourier integral operator; consequently we form a phase-space image as a filtered adjoint of this operator or weighted matched filter.

The theory allows for activation of multiple transmitters at different times, but the theory is simpler when they are all activated so that the waves arrive at the target at roughly the same time.

We conclude that a single kind of high range-resolution waveform should be avoided if both the position and the velocity are to be reconstructed. Furthermore, we see that a single kind of high range-Doppler waveform can reconstruct not only the velocity but also the position. This may be related to the theory of Doppler SAR imaging [23].

We leave for the future an investigation of the effect of relative waveform power on the imaging results.

VII. Acknowledgements

We are grateful to the Air Force Office of Scientific Research[1] for supporting this work under agreement FA9550-09-1-0013, and to the China Scholarship Council for supporting L.W.'s stay at Rensselaer.

References

[1] C. E. Cook and M. Bernfeld, *Radar Signals*, Academic: New York, 1965.

[1]Consequently the U.S. Government is authorized to reproduce and distribute reprints for Governmental purposes notwithstanding any copyright notation thereon. The views and conclusions contained herein are those of the authors and should not be interpreted as necessarily representing the official policies or endorsements, either expressed or implied, of the Air Force Research Laboratory or the U.S. Government.

[2] P. M. Woodward, *Probability and Information Theory, with Applications to Radar*, McGraw-Hill: New York, 1953.
[3] N. Levanon, *Radar Principles*, Wiley: New York, 1998.
[4] N. J. Willis, *Bistatic Radar*, Artech House: Norwood, MA, 1991.
[5] N. J. Willis and H. D. Griffiths, *Advances in Bistatic Radar*, SciTech Publishing: Raleigh, NC, 2007.
[6] N. J. Willis, *Bistatic Radar in Radar Handbook (by M. I. Skolnik, 2nd Edition)*, McGraw-Hill: New York, 1990.
[7] T. Tsao, M. Slamani, P. Varshney, D. Weiner, H. Schwarzlander, and S. Borek, "Ambiguity function for a bistatic radar," *IEEE Transactions on Aerospace and Electronic Systems*, vol. 33, pp. 1041–1051, 1997.
[8] B. Himed, H. Bascom, J. Clancy, and M. C. Wicks, "Tomography of moving targets (tmt)," in *Sensors, Systems, and Next-Generation Satellites V., Proceedings of SPIE*, 2001, vol. 4540, pp. 608–619.
[9] I. Bradaric, G. T. Capraro, D. D. Weiner, and M. C. Wicks, "Multistatic radar systems signal processing," in *Proceedings of IEEE Radar Conference 2006*, 2006, pp. 106–113.
[10] I. Bradaric, G. T. Capraro, and M. C. Wicks, "Waveform diversity for different multistatic radar configurations," in *Proceedings of Asilomar Conference*, 2007.
[11] R. S. Adve, R. A. Schneible, M. C. Wicks, and R. McMillan, "Adaptive processing for distributed aperture radars," in *Proceedings of 1st Annual IEE Waveform Diversity Conference, Edinburgh*, Nov. 2004.
[12] R. S. Adve, R. A. Schneible, G. Genello, and P. Antonik, "Waveform-space-time adaptive processing for distributed aperture radars," in *2005 IEEE International Radar Conference Record*, 2005, pp. 93–97.
[13] L. Landi and R. S. Adve, "Time-orthogonal-waveform-space-time adaptive processing for distributed aperture radars," in *2007 International Waveform Diversity and Design Conference*, 2007, pp. 13–17.
[14] G. T. Capraro, I. Bradaric, D. D. Weiner, J. Parretta R. Day, and M. C. Wicks, "Waveform diversity in multistatic radar," in *International Waveform Diversity and Design Conference, Lihue, HI*, Jan. 2006.
[15] D. Colton and R. Kress, *Inverse Acoustic and Electromagnetic Scattering Theory*, Springer, 1992.
[16] A. J. Devaney, "Inversion formula for inverse scattering within the born approximation," *Optics Letters*, vol. 7, pp. 111–112, 1982.
[17] A. J. Devaney, "A filtered backpropagation algorithm for diffraction tomography," *Ultrasonic Imaging*, vol. 4, pp. 336–350, 1982.
[18] T. Varsolt, B. Yazici, and M. Cheney, "Wide-band pulse-echo imaging with distributed apertures in multi-path environments," *Inverse Problems*, vol. 24, no. 4, pp. 045013 (28 pp.), Aug. 2008.
[19] M. Cheney and B. Borden, "Imaging moving targets from scattered waves," *Inverse Problems*, vol. 24, pp. 035005(1–22), 2008.

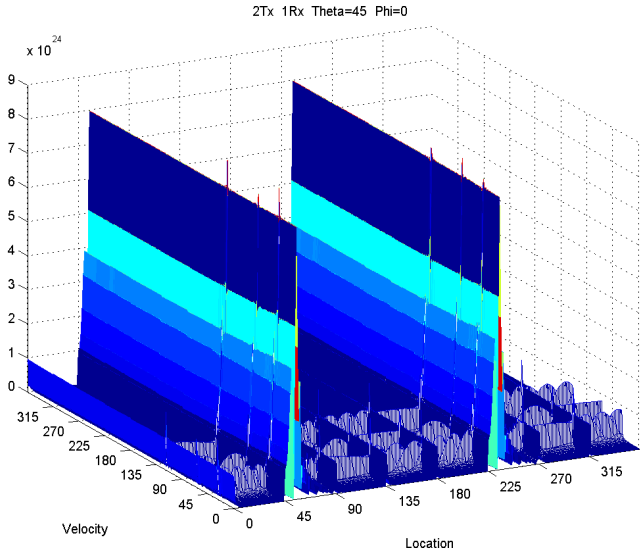

Fig. 5: This shows the combined point-spread function for the two-transmitter, single-receiver case, when the transmitter on the x axis transmits waveform 1 and the transmitter on the y axis transmits waveform 4.

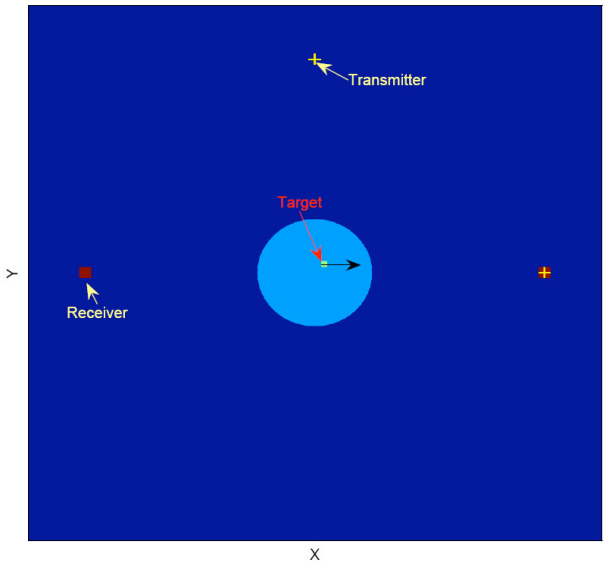

Fig. 6: This shows the geometry for the two-transmitter, two-receiver case, together with the target and region of interest (not to scale).

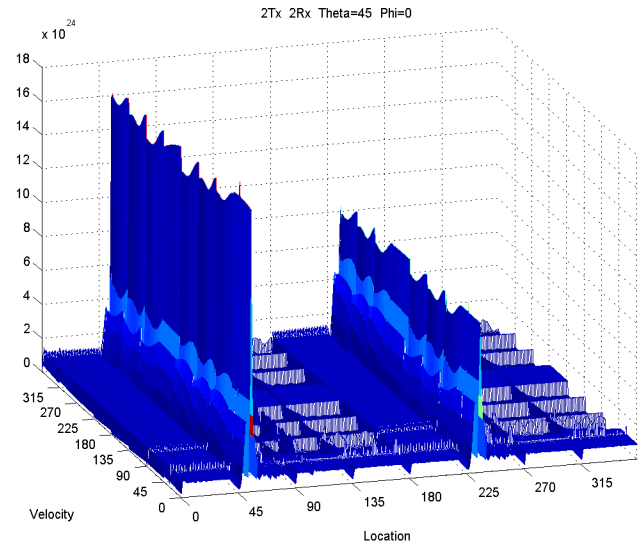

Fig. 7: This shows the combined point-spread function for the two-transmitter, two-receiver case, when the transmitter on the x axis transmits waveform 1 and the transmitter on the y axis transmits waveform 4.

[20] C. J. Nolan and M. Cheney, "Synthetic aperture inversion," *Inverse Problems*, vol. 18, pp. 221–236, 2002.

[21] N. Bleistein, J. K. Cohen, and J. W. Stockwell, *The Mathematics of Multidimensional Seismic Inversion*, Springer: New York, 2000.

[22] B. Yazici, M. Cheney, and C.E. Yarman, "Synthetic-aperture inversion in the presence of noise and clutter," *Inverse Problems*, vol. 22, pp. 1705–1729, 2006.

[23] B. Borden and M. Cheney, "Synthetic-aperture imaging from high-doppler-resolution measurements," *Inverse Problems*, vol. 21, pp. 1–11, 2005.

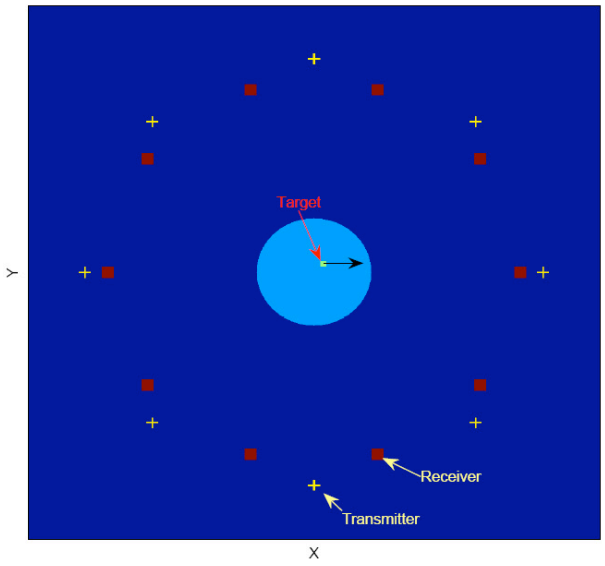

Fig. 8: This shows the circular geometry (not to scale).

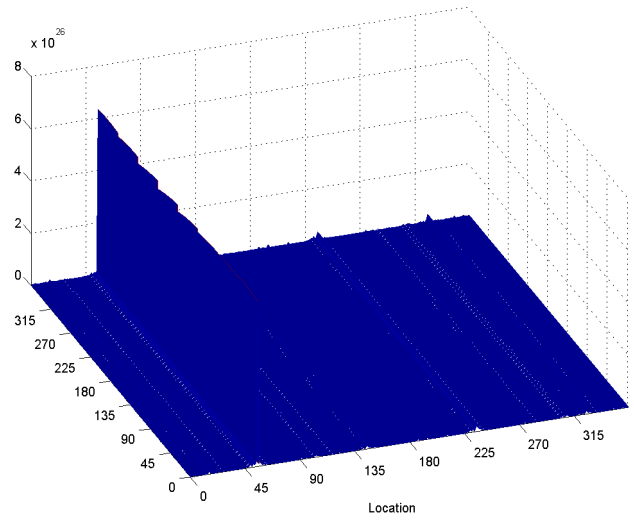

Fig. 9: This shows the combined point-spread function for the circular geometry when all transmitters are transmitting waveform 1.

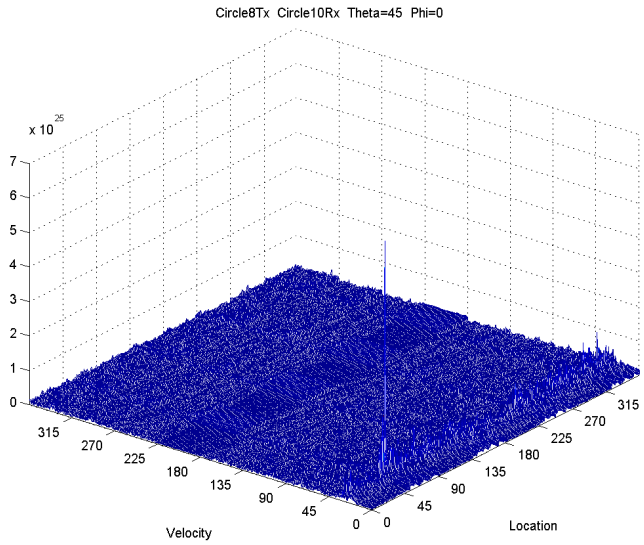

Fig. 10: This shows the combined point-spread function for the circular geometry when all transmitters are transmitting waveform 4

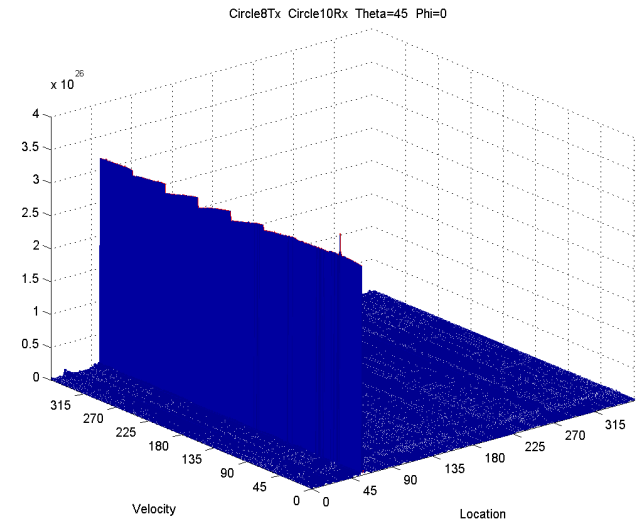

Fig. 11: This shows the combined point-spread function for the circular geometry when every other transmitter transmits waveform 1, and the others transmit waveform 4.